Journal of Maps

ISSN: (Print) (Online) Journal homepage: https://www.tandfonline.com/loi/tjom20

Geomorphology of the high-elevated flysch range – Mt. Babia Góra Massif (Western Carpathians)

Piotr Kłapyta

To cite this article: Piotr Kłapyta (2020) Geomorphology of the high-elevated flysch range – Mt. Babia Góra Massif (Western Carpathians), Journal of Maps, 16:2, 689-701, DOI: 10.1080/17445647.2020.1800530

To link to this article: https://doi.org/10.1080/17445647.2020.1800530

JOURNAL OF MAPS
2020, VOL. 16, NO. 2, 689–701
https://doi.org/10.1080/17445647.2020.1800530

Taylor & Francis
Taylor & Francis Group

Science

Geomorphology of the high-elevated flysch range – Mt. Babia Góra Massif (Western Carpathians)

Piotr Kłapyta

Faculty of Geography and Geology, Institute of Geography and Spatial Management, Jagiellonian University, Kraków, Poland

ABSTRACT

A detailed geomorphological map of the Mt. Babia Góra Massif (1725 m a.s.l.), at a scale 1:10,000 is presented. A slope, glacial, periglacial and fluvial features were mapped on the base of the coupled field studies and LiDAR DEM analyses. This study underlines the complexity of rock slope failures (RSFs), in shaping the morphology of compact and isolated upland, exhibiting one of the highest incidences of RSFs yet recorded in Europe (29% for a whole massif, and 45% for the north face). A total of 212 RSFs were mapped of which 18 failures are large landslides (>0.25 km^2), among them is one of the largest known (2.6 km^2 and 150 × 106 m^3) in the Polish Flysch Carpathians. The mapping and Schmidt-hammer results shed light on the problem of glacial relief of the massif, documenting the remnants of glacial deposits beyond the tongues of landslides in the Szumiąca Woda valley.

ARTICLE HISTORY
Received 27 April 2020
Revised 21 July 2020
Accepted 21 July 2020

1. Introduction

The Western Carpathians are characterised by frequent occurrences of various types of slope failures (Němčok, 1982; Ondrášik, 2002). Large rock slope failures (RSF) including ridge-splitting slope deformations, rock avalanches and rockslides are widespread on various lithologies in the high-elevated Tatra Mountains (2655 m a.s.l.) and Low Tatra Mountains (2043 m a.s.l.) (Němčok, 1982; Pánek et al., 2016) (Figure 1(a)). The largest number and density of mass movements are however associated with moderate-relief dominated landscape of the Outer Western Carpathians (Flysch Carpathians) (Figure 1(a)), which are known as one of the most landslide-prone regions in Europe (Margielewski, 2006a; Mrozek et al., 2014; Pánek et al., 2019). Landforms in the Outer Western Carpathians are strongly influenced by geological structure, dominated by thrusted-and-folded sequences of turbiditic rocks (flysch) (Margielewski, 2006a, 2006b). Because of predominant northward vergence of tectonic units, monoclonally arranged flysch morphostructures are common in this area (Margielewski, 2006a; Březný & Pánek, 2017). The small (72 km^2) Mt. Babia Góra Massif (Figure 1) represents the highest part of the Outer Western Carpathians (1725 m a.s.l.), featuring prominent local topography (up to 1095 m relief) and structural asymmetry between steep north-facing escarpment slope and gentle south-facing dip slopes (Figure 1(b)).

Because of the forested nature of the Flysch Carpathians, gravity-induced landforms are covered by vegetation and thus regional-scale landslide inventories are quite recent and based on systematic field mapping (e.g. SOPO Project; Mrozek et al., 2014) and LiDAR-based mapping. Recent mass movements inventories led to the discovery of approximately 60,000 objects in the Polish part (Mrozek et al., 2014), and over 13,600 landslides in the Czech part of the Outer Western Carpathians (Pánek et al., 2019). Although the presence of slope failures on the Mt. Babia Góra has been noted for over 100 years (Alexandrowicz, 1978; Łajczak, 2014; Rehman, 1895; Zapałowicz, 1880; Ziętara, 2004; Ziętara & Ziętara, 1958), the lack of high-resolution topographic data significantly constrained landform recognition and mapping. Deep landslide scars and trenches are clearly visible above the tree line, however, entire landslide distribution and extent were widely undetected due to their occurrence on steep slopes on inaccessible mountain terrain covered with dense forest or shrub pine cover. Recently, new features of landslide relief were discovered using LiDAR data in selected test areas (Kłapyta & Kolecka, 2015; Łajczak et al., 2014).

Due to high altitude and location close to the northern fringe of the Carpathians, in a periglacial corridor between the Fennoscandian ice sheet and the ice masses of the Alps (Heyman et al., 2013), there were potentially suitable conditions for local glaciation in the Babia Góra during the Quaternary. The presence

CONTACT Piotr Kłapyta piotr.klapyta@uj.edu.pl Faculty of Geography and Geology, Institute of Geography and Spatial Management, Jagiellonian University, ul. Gronostajowa 7, 30-387 Kraków, Poland

Supplemental data for this article can be accessed at https://doi.org/10.1080/17445647.2020.1800530

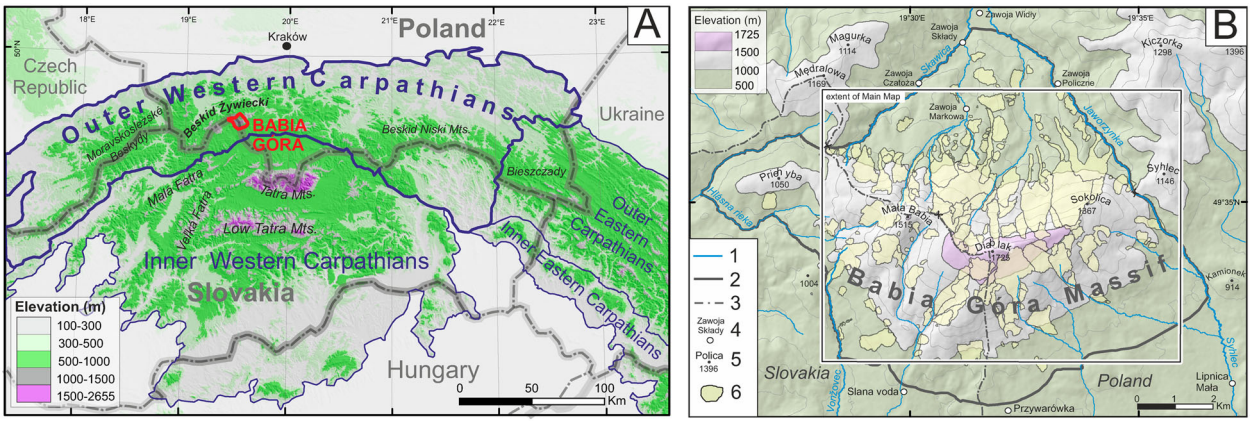

Figure 1. Location of the study area. (A) Position of the study area in the Western Carpathians. (B) Location and borders of the Babia Góra Massif to the Main Map extent. (1 – Main streams, 2 – Borders of the Babia Góra Massif, 3 – National border, 4 – Settlements, 5 – Summits, 6 – Landslides)

of glacial landforms and sediments has been vigorously discussed. The early concept of the presence of an extensive ice cap during the Riss and cirque glaciers during the Würm glaciation (Sawicki, 1913) was largely rejected by further studies on the basis of the landslide genesis of many scars and hummocky boulder deposits (Alexandrowicz, 1978; Starkel, 1960; Ziętara, 1962; Ziętara & Ziętara, 1958). Nonetheless, the glaciation hypothesis was still accepted by some authors (Klimaszewski, 1952; Książkiewicz, 1963; Niemirowski, 1963), but has evolved into two concepts according to which glacial landforms are (i) older and subsequently modified by large scale paraglacial mass movement processes (Książkiewicz, 1963, 1966; Niemirowski, 1963; Wójcik et al., 2010), or (ii) younger than large Neogene-early Quaternary age landslides and that some of their scarps have been glacially remodelled (Łajczak, 1998, 2014).

The aim of this study is to present the first detailed geomorphological map of the entire Babia Góra Massif, based on combination of extensive field landform inventory mapping and LiDAR data analysis. These data allow for the first time to create a comprehensive picture of landform assemblages in this area with the special attention to the geomorphic imprint of RSFs. A combination of geomorphological mapping with relative age dating and sedimentological analysis sheds new light on relations between mass movement and glacial features in the Babia Góra Massif.

2. Methodology

Geomorphological mapping encompassing 80% (~57 km^2 on a Main Map) of the Babia Góra Massif (72 km^2) was made by integrating both detailed field landform inventory and remote sensing techniques. The boundaries of the massif were defined according to Łajczak (2016) (Figure 1(b)). Due to its shape (9.4 × 4.1 km), the Main Map excludes external, low-relief part of the massif with single occurrence of mass movements (Figure 1(b)). These landforms were included in the calculation of total area affected by RSFs. Detailed field mapping at 1:5000 scale was carried out over a five-year period (2013–2018) and was complemented by analysis of high-resolution (1 × 1 m) airborne LiDAR-derived Digital Elevation Model (DEM) and colour orthophotos taken by the Centre for Geodesy and Cartography of Małopolska council in 2002, with a pixel size of 25 cm.

All geomorphological features were identified and manually digitised employing on-screen mapping using LiDAR-derived hillshade, slope and contour (contour interval of 2 m) as a base map created in ArcGIS software. Mapping was also supported by comparison with previous geological and geomorphological maps (Alexandrowicz, 2004; Golonka & Wójcik, 1976; Książkiewicz, 1971, 1983; Teťák et al., 2016; Wójcik et al., 2010), which were scanned, georeferenced, and critically analysed by comparing them with field results and remote sensing data.

Mapped landforms have been divided into four different morphogenetic systems: slope, glacial, periglacial, and fluvial. The Rock slope failure (RSF) classification of Jarman (2006) and Jarman and Harrison (2019), embracing rockslides, rock avalanches and rock slope deformations, was adopted in the mapping. Because flow-like forms are integral part of the rockslides, they were mapped as a one type. A threshold size of 0.25 km^2 for large landslides was adopted according to Jarman (2006), whereas the lowest identified size was 0.0003 km^2. RSFs morphology was defined by the occurrence of typical diagnostic features for mass movements as: scarps, tension cracks, irregular 'hummocky' terrain with bulges and toes and slide or backward rotated blocks (Březný & Pánek, 2017; Van Den Eeckhaut et al., 2012).

Because moraines are hardly distinguished from landslide deposits based solely on surface morphology, additional field analyses including clast shape and roundness measurements for 50 clasts at each site

(Benn & Ballantyne, 1994) together with Schmidt hammer (SH) relative age dating (Shakesby et al., 2006) were performed in the Szumiąca Woda valley, where previous research indicated the presence of glacial landforms. The SH measurements followed the methodology of Matthews and Shakesby (1984). Thirty hammer impacts were recorded per boulder from a total of five boulders at each of 25 measurement sites, and the mean rebound value was calculated. The rebound values (R-values) tend to decline in response to rock-surface weathering and hence they reflect the time for which the rock surface has been exposed to subaerial processes (Kłapyta, 2013; Matthews & Shakesby, 1984).

The main map layout is at 1: 10,000 scale when printed on A0 sheet. The background shaded relief map and 25 interval contours generation were derived from the DEM and performed in ESRI ArcGIS, where also further landform recognition and interpretation were carried out (ESRI, 2016). The digitised vector files for the base data were converted from ArcGIS format and importing into CorelDRAW, where final map processing was performed.

3. Study area

The Babia Góra Massif is the highest mountain range in the Outer Western Carpathians (Diablak, 1725 m a.s.l.; 49°34'23''N; 19°31'46''E), located close to the northern fringe of the Carpathians, at the border between Poland and Slovakia. The study area is a part of the thrust-and-fold belt of the Flysch Carpathians formed by the Magura unit, which consists of ca 2 km thick sequence of Upper Cretaceous-Eocene flysch rocks dipping gently (ca 20°) towards the S and SW (Książkiewicz, 1971, 1983) (Figure 2). Flysch bedrock is affected by joint and fault sets running in NE-SW, SE–NW and ENE–WSW directions (Aleksandrowski, 1985; Łajczak, 2014). These discontinuities define the boundaries of the Massif and the large rock mass movements (Figure 1(b)). According to recent findings (Jankowski et al., 2019; Jankowski & Margielewski, 2014), the local topography of the Babia Góra Massif was associated with Late Miocene orogenic collapse and gravitational displacement of large blocks southward from the Babi Góra Massif along normal faults. As a result of significant unloading, the core zone of the Massif located at the footwall of the normal fault became intensive isostatically elevated (Jankowski & Margielewski, 2014). A deep tectonic zone bounding the southern slope of the Babia Góra is underlined by the zone of triangular facets and linear concentration of mineral springs along the supposed fault zone (Łajczak, 2016) (Figure 1(b)).

Landforms within the study area are strongly influenced by geological structure (Łajczak, 2013, 2014). The main 10 km long ridge of the Babia Góra Massif of coherent Magura-type thick sandstone cap that overlie strongly folded, weak claystone/siltstone-dominated flysch of sub-Magura beds at the northern, and chaotic complexes (tectonic melange) at the southern foreland (Jankowski & Margielewski, 2014). Steep (40°–78°) northern anaclinal/escarpment slopes form typical cuestas with local rock walls and concave profiles that are presently affected by shallow rockslides, rock falls, modern and relict debris flows and snow avalanches (Czajka et al., 2015; Łajczak, 2016). Southern dip (cataclinal) slopes with a shallower gradient (20°–40°) and convex-concave profiles show translational rockslides (Łajczak, 2014) that are strongly influenced by geological structure (Figure 2(b)). With respect to historical and modern activity of gravity-induced slope deformations (Łajczak & Migoń, 2002; Midowicz, 1974), the study area shows higher frequency events compared with adjacent parts of Western Carpathians with the rigid thick-bedded flysch. The western part of the Massif of the Mała Babia Góra (1515 m a.s.l.), features deeply-incised valleys with headwaters located just below the main ridge, which contrasts with the eastern part (Diablak 1725 m a.s.l.), dominated by relatively shallow and short valleys with low-elevated headwaters located at 900–1200 m on the northern, and 1200–1400 m on the southern slopes (Łajczak, 2014).

Due to the topographic barrier Babia Góra is one of the wettest locations in the Western Carpathians, with high orographically induced annual precipitation exceeding 1450 mm and maximum daily intensity of 234 mm at the northern slopes (Obrębska-Starklowa, 2004). The predominant wind direction is NW in summer and SW during winter (Obrębska-Starklowa, 2004). Forests reach up to approximately 1370 m a.s.l. (Czajka et al., 2015) and dwarf pine up to 1650 m a.s.l. Although the mean annual air temperature in the summit area is below 0°C (Obrębska-Starklowa, 2004), no evidence of contemporary permafrost exists (Dobiński et al., 2016). The Babia Góra National Park contains a Polish part of the Massif and has been also declared as Biosphere Reserve by UNESCO in 1977.

4. Results

4.1. Slope and slope landforms

In the study area, slopes and slope covers are strongly influenced by the flysch bedrock and thus in this map, two types of slopes were distinguished according to the extent of thick-bedded Magura sandstones and claystone/siltstone dominated Sub-Magura beds (Figure 2). Blocky and debris slope covers are typical of rigid thick-bedded sandstone, whereas muddy covers come from weak claystone formations. Solid

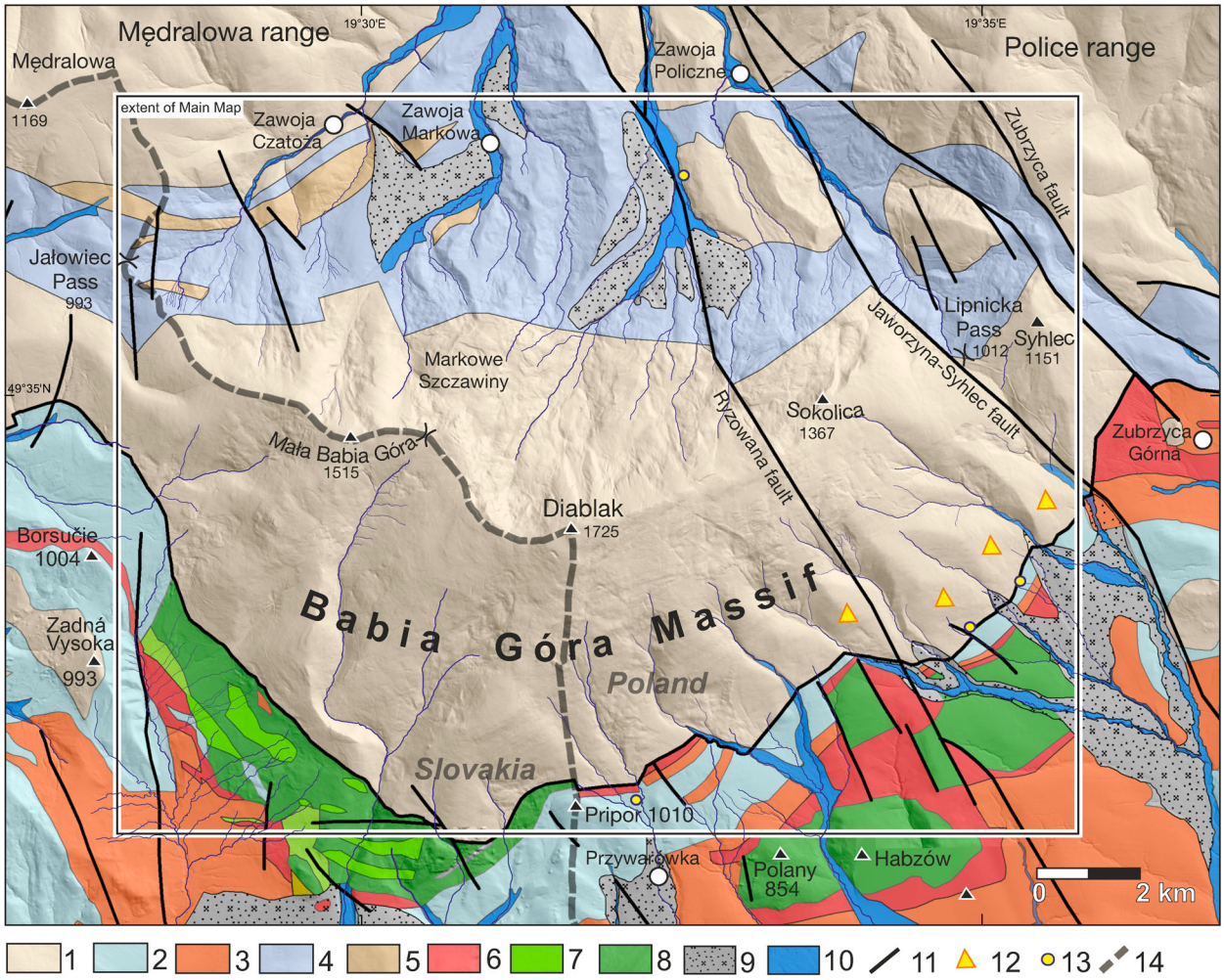

Figure 2. Geological map of the Babia Góra Massif based on Książkiewicz (1971, 1983); Aleksandrowski (1985); Teťák et al. (2016) and Geological Map of the Slovak Republic 1:50,000. Legend: 1 – Magura beds; thick-bedded sandstone-dominated flysch sequence (Upper Eocene); Sub-Magura beds: 2 – Bistrica beds; thin-bedded flysch and marls (Middle Eocene), 3– Beloveža Beds; thin-bedded flysch (Middle Eocene), 4 – Hieroglyphic Beds; thin-bedded flysch (Middle Eocene), 5 – Osielec sandstones (Eocene), 6 – Variegated shales, red and variegated shales (Paleocene–Eocene), 7 – Ropianka Beds; thin- and medium-bedded flysch (Late Cretaceous–Paleocene), 8 – Szczawina sandstones; thick-bedded sandstones and conglomerates (Late Cretaceous), 9 – Alluvial cones (Pleistocene), 10 – River terrace (Holocene), 11 – Faults, 12 – Triangular facets, 13 – Mineral springs, 14 – National border.

bedrock is only locally exposed along the main ridge, in rocky landslide scarps and along river channel undercuttings and in rock steps up to 4.5 m in high forming waterfalls (Figure 3).

Geomorphological mapping revealed relict and modern debris flow tracks on the northern slopes of the Babia Góra Massif. A total number of 24 fossil and 3 modern tracks (Figure 4(a)) were identified below Mt. Diablak and Gówniak within the altitudinal belt 1200–1680 m. The mean length of individual fossil debris flow tracks is 630 m and maximal length reaches approximately 1 km. They occur on steep slopes (20°–34°) with local maximal inclination up to 70°. Debris flow tracks from 3 to 4 m deep gullies (Figure 4(b)) in the erosional zone, and fossil debris accumulation up to ~3 m thick and ~5–35 m wide in the deposition zone which form lateral levees, that pass downslope into torrent cones. Modern tracks were triggered by heavy rainfall in 1997, 2002 and 2004 (Łajczak et al., 2015) and the longest track reaches 760 m (Łajczak & Migoń, 2002; Matyja, 2006) (Figure 4(a)).

RSFs are the most important landscape forming features in the Babia Góra Massif. The total area affected by RSFs is 20.4 km^2 (28.7% of the study area) (Figure 5, Table 1). A total of 212 failures in the Babia Góra Massif were mapped, 84% being rockslides, 9% rock slope deformations, and 7% rock avalanches. Rockslides are characterised by clear cavities and slipmass involving multiple block displacements in the upper section (Figure 6(b)), and a bulged toe in the lower portion. Some of the rockslides have evolved into complex flow-like forms (Cruden & Varnes, 1996; Pánek et al., 2013), with elongated depositional bodies (Figure 6(a)), resulted from collapse, liquefaction and flow within incompetent sub-Magura beds. The distal earthflow tongues extending over relatively long distances (450–1650 m) have fully infilled the valley floor and significantly influenced their topography. They contain poorly sorted diamict

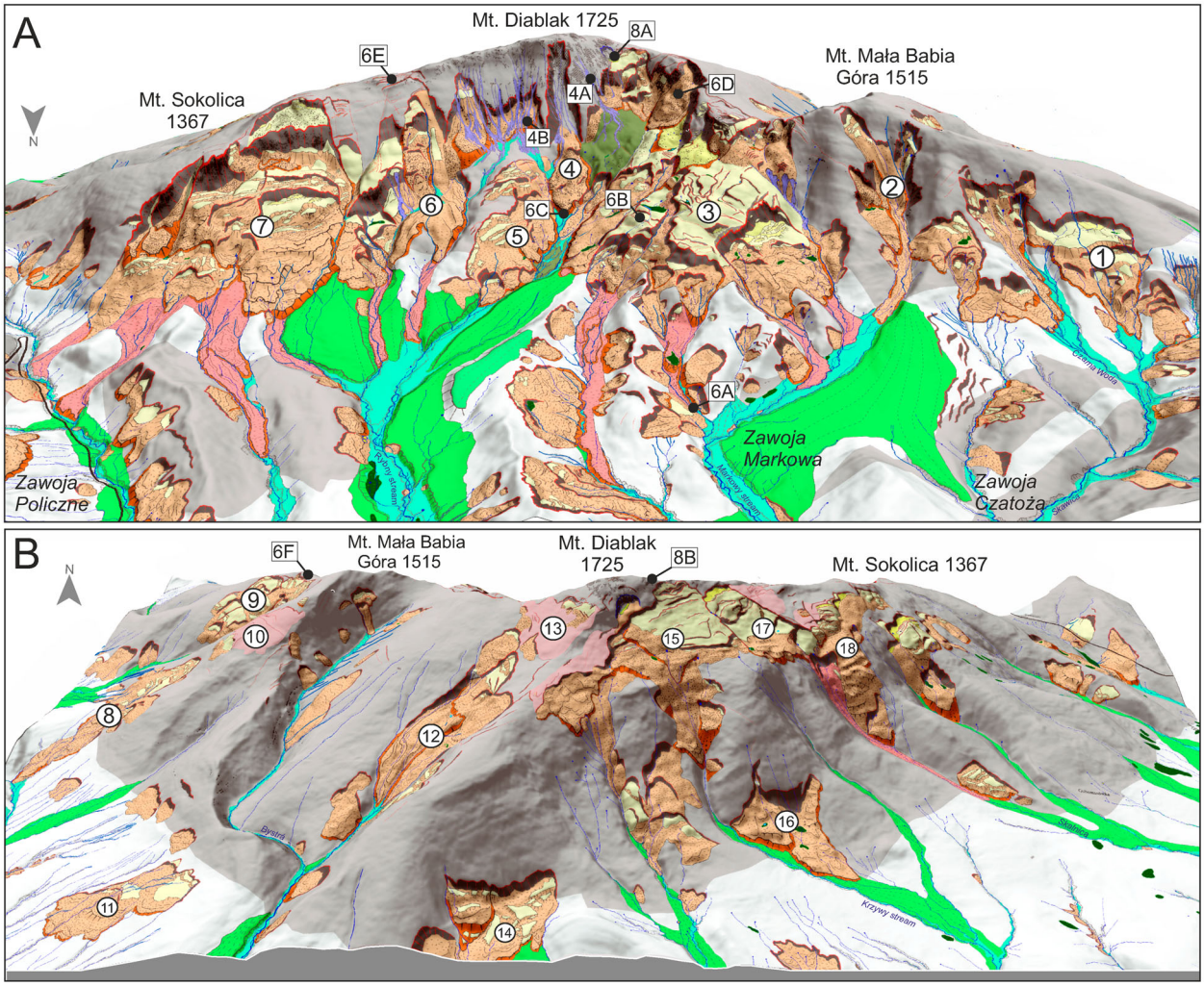

Figure 3. Morphological asymmetry of the Babia Góra Massif. (A) North-exposed escarpment slope, (B) South-exposed dip slope. Main Map projected on the LiDAR DTM. White circles refer to the location and number of large rock slope failures, its morphometrical characteristics are presented in Supplementary Data 1. Symbols in squares refer to the location of landforms presented in Figures 4, 6 and 8.

sediments with allochthonous Magura sandstone boulders (Figure 6(a)).

Rock avalanches (Figure 5, Table 1) occur in the upper section of the Babia Góra northern slope (1300–1500 m a.s.l.), with the highest slope gradients (40°–70°). These failures have striking rocky cavities and debris lobes of disintegrated, openwork angular debris (Figure 6(d)). The morphology, blocky character

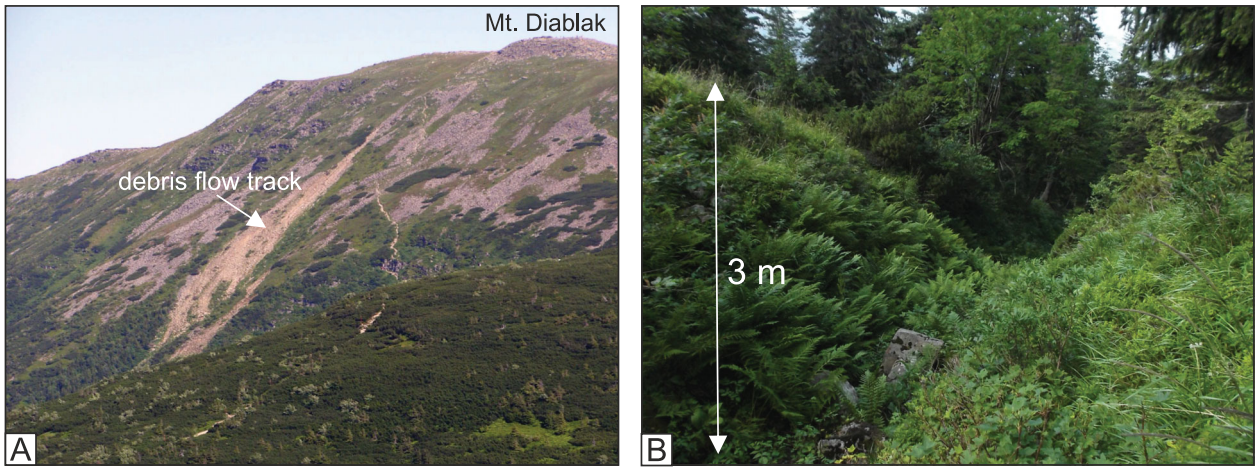

Figure 4. Hillslope landforms in the Babia Góra Massif. (A) The longest (760 m) modern debris flow track formed in 2002 on the northern slope of the Babia Góra Massif. (B) Relict debris flow gully at Urwisko site.

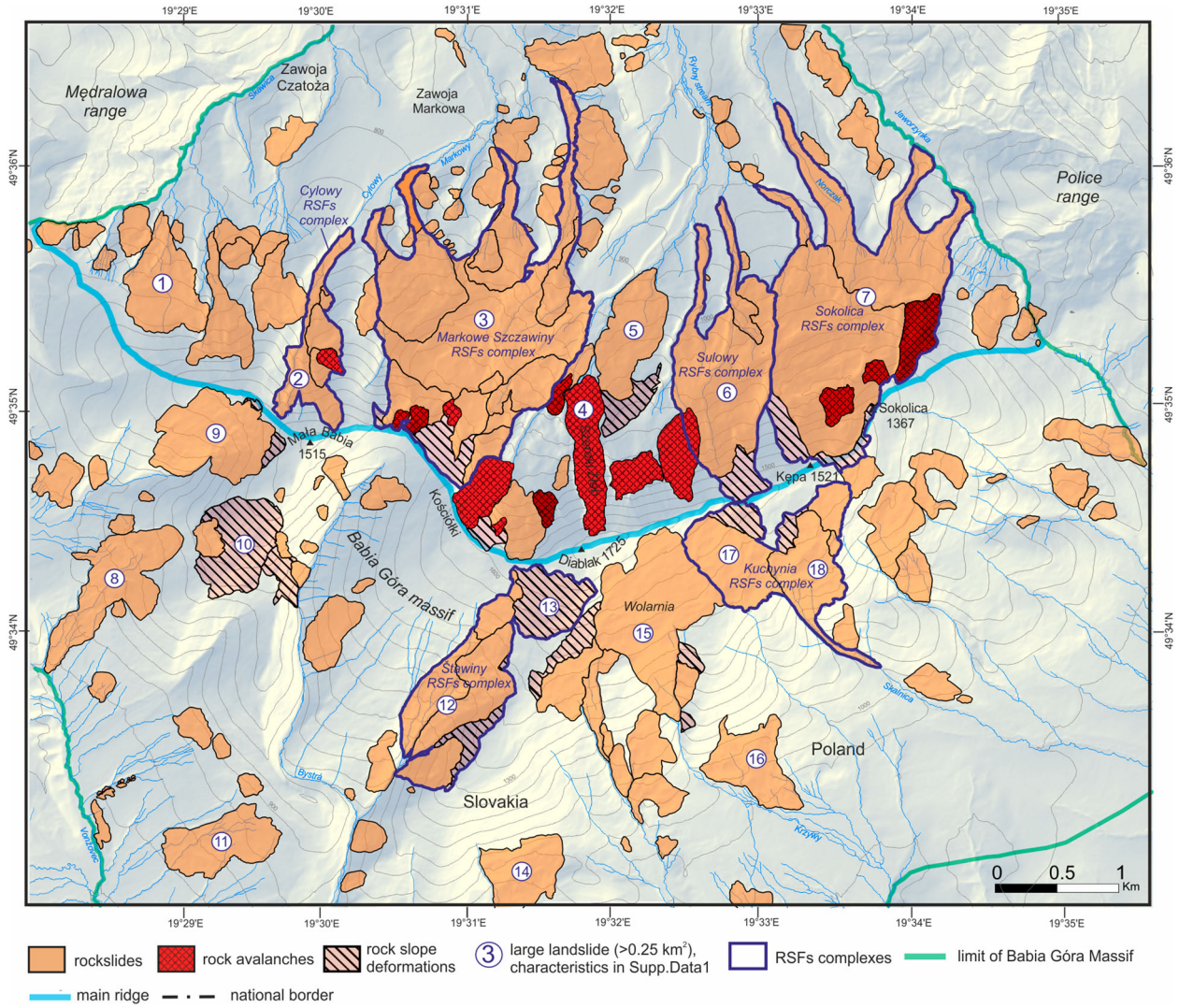

Figure 5. RSF inventory map of the Babia Góra Massif.

of the material and similar SH R-values (Supplementary data 2) indicate single and rather sudden origin of these failures.

Rock slope deformations (RSD; Agliardi et al., 2001; Jarman, 2006; Pánek & Klimeš, 2016) were recognised in the ridge-top area of Babia Góra Massif, above scarps of large rockslides, marking retrogression to the crest. RSD are characterised by diffuse margins (Jarman & Harrison, 2019) and occurrence of fissures, tension cracks, ridge-top trenches with crevice type caves, steep like arranged uphill and downhill-facing scarps (Figure 6(e,f)), which resulted from deep-reaching slope extension, opening of joints and short horizontal displacements. A total of 20, small (up to

Table 1. RSFs size data for the Babia Góra Massif.

		Massif	N slope	S slope
Number of RSFs		212	125	87
Total RSF area (km^2)		20.4	12.02	8.38
Total massif area (km^2)		71.74	26.76	44.98
RSF/massif %		28.7	44.9	18.6
RSF density (RSF/km^2)		3	4.6	1.9
Rockslides	Number	178	103	75
	Area (km^2)	17.45	10.19	7.26
Rock avalanches	Number	15	15	–
	Area (km^2)	1.27	1.27	–
Rock slope deformations	Number	19	7	12
	Area (km^2)	1.68	0.56	1.12
Large RSFs	Number / % of total	18/ 8.5	7/5.6	11/10.3
	Area (km^2)/% of total	12.2/60	7.4/61	4.8/ 52
Complexes	Number	6	4	2
	Area (km^2)	8.82	6.74	2.08

Figure 6. Rock slope failures in the Babia Góra Massif. (A) Front of a complex flow-like rockslide in the Barańcowy stream valley. Angular sandstone debris at the surface of a flow-like landform. (B) Tilted translated block of the Markowe Szczawiny rockslide. (C) Distinct, 30 m high front of the Szeroki Żleb rock avalanche. (D) Debris field of the Kościółki rock avalanche. (E) Rock slope deformations (RSD) at Zimna Dolinka site. (F) Extensional trench with the entrance to the Złota Studnia crevice-type cave in the upper part of the Hlasna rieka RSD.

86 m in length) crevice caves were recognised in the Massif.

A total of 125 RSFs occur on the north-exposed escarpment slope, where the highest overall landslide area (12 km^2) and RSF density (4.6/km^2) are also found (Table 1). The northern slope area features the highest local relief and slope gradients (40°–70°) and suitable structural conditions for sliding. This is well expressed in the exceptionally high incidences of slope failure (44.9%), which is more than two times larger when compared to south dip slope (Figures 4 and 5; Table 1). The elevation belt 920–1500 m a.s.l. is preferred for mass movements on the northern slope, showing values above the mean (Figure 7(b)), however, the most pronounced cluster of RSFs is at the altitudinal range 950–1150 m, where more than 70% of the area is affected by mass movements (Figure 7). RSF scarps on the northern slope (38%) cluster between 800 and 1040 m which corresponds to the rockslides on the valley-sides and in the headwaters (Łajczak, 2014).

In contrast, on southern/dip slopes, RSFs cluster in the higher elevation belt between 1200 and 1650 m, where more than 40% of the area is affected by mass movements (Figure 5). The largest concentration of RSFs occurs in headwater areas at 1200–1300 m and 1400–1470 m (Łajczak, 2014) (Figure 7). The cluster at 1500–1650 m corresponds to relatively shallow but extensive structural translational rockslides and rock slope deformations along gentle dipping bedding planes (<20°).

Average RSF size is 0.10 km^2, however, the size distribution of RSFs in the Babia Góra Massif is dominated by large landslides (>0.25 km^2), that cover 60% of the total area affected by RSFs (Figure 5, Supplementary data 1) and represent 8.5% of their total number (Table 1). A total of 18 large landslides could be classified as largest scale slope deformations, with volumes larger than 5×10^6 m^3 (Fell, 1994) (Supplementary data 1). Large landslides are relatively uniformly distributed on the anticlinal and cataclinal slopes, however, on the northern slope, they comprise up to 61% of the total landslide area, as well as three of the largest RSFs in the study area (Table 1, Supplementary data 1).

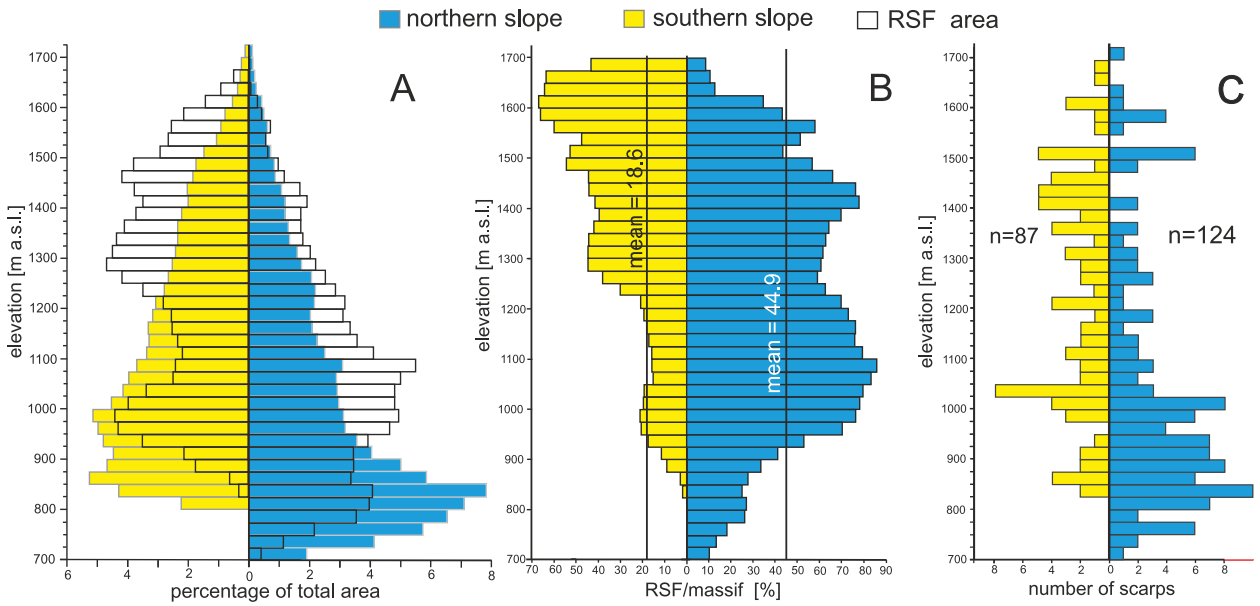

Figure 7. Rock slope failure area for the altitude in the Babia Góra Massif. (A) Distribution of altitude within RSF terrain and all massif area (B) Ratio of the landslide area within each class for altitude (C) Maximum altitude of landslide scarp areas.

Six examples of complex RSFs (Cruden & Varnes, 1996) were distinguished in the study area (Figure 5, Table 1), and display evolution from deformation to sliding and collapse/flow. This are the largest (4.6–164.3 × 10^6 m^3) gravity-induced slope deformations in the Babia Góra Massif, covering the middle and lower portions of the northern slopes. Among them are one of the largest known failures in the Polish part of the Outer Western Carpathians – the Markowe Szczawiny landslide complex (2.6 km^2 area, 164.3 × 10^6 m^3 in volume) (Table 1; Supplementary data 1). The landslide complexes shows an exceptionally large height with an elevation difference of approximately 880 m between the back wall and leading edge of the accumulation area, and extensive maximal sliding distance of approximately 3.2 km, which is larger than the longest known landslide in the Polish part of the Outer Western Carpathians (Mrozek et al., 2014).

4.2. Periglacial and glacial landforms

The landscape of the highest Babia Góra massif has been affected by periglacial processes. Blockfields and blockstreams cover ca 1.85 km^2 of the study area and represent cold-climate periglacial landforms developed in Magura-type sandstones (Figure 8(a)). Block covers are 1–2 m thick, of in situ block mantles with ca 30% of fine matrix (Łajczak & Włoch, 2004; Ziętara, 1989, 2004) and are mostly concentrated on northern slopes (72% of the total area) in the altitudinal range 1425–1725 m. Blockfields are relict (Klimaszewski, 1948, 1952; Łajczak, 2013), however, evidence of current build up by mechanical weathering of sandstone was also documented (Jahn, 1958). On the high gradient slopes, elongated blockstreams were formed as the result of slow creep. Step-like cryoplanation terraces with gently sloping treads and rubble-covered scarps related to outcrops of sandstone beds were identified along the main ridge area between Mt. Kępa and Mt. Kościółki. Small (1–2 m high) relict pronival ramparts and shallow nivation hollows have been identified in the highest part of the Massif, around Mt. Diablak (1725 m) (Figure 8(b)).

Glacial sediments in the Babia Góra Massif were distinguished by sedimentological analyses (clast shape and roundness; Figure 9(b)), presence of large (>2 m) sub-rounded boulders (Figure 9(e)), as well as SH measurements (Figure 9(a,c), Supplementary data 2), which indicate clear differences between moraines and adjacent landslide and fluvial deposits. Moraines are preserved exclusively on the northern slopes of Mt. Babia Góra beyond the limits of landslide tongues in two discontinuous locations in the upper (1375–1160 m) and lower part (915–990 m) of the Szumiąca Woda valley (Figure 8(a,e)). The first area shows a glacial cirque with low-relief moraine cover with large (up to 4–5 m) sandstone boulders (Książkiewicz, 1963; Łajczak, 1998) resting on a matrix-supported diamicton with sub-rounded and rounded clasts (Figure 9(b)). In the lower part of Szumiąca Woda valley moraines are traced as isolated patches of till without moraine ridges, which were eroded by river channel avulsion and buried by proximal outwash fans. Erosion is an effect of local site conditions, especially exposure of glacial deposits to high energy fluvial and mass movements (Kirkbride & Winkler, 2012). A 5 m high morphological step in the longitudinal valley profile is formed by large boulders (Figure 9(e)) lacking in adjacent landslide deposits. SH-rebound values indicate an old relative age of the moraines (R = 30–32), similar to periglacial block covers (R = 30) and slightly older than pronival ramparts (R = 33), but significantly

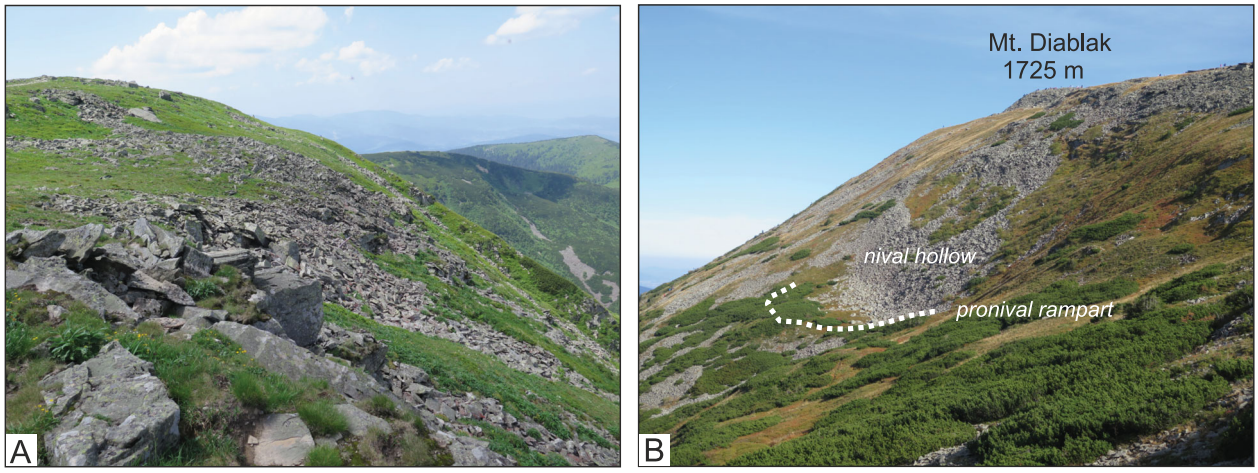

Figure 8. Periglacial landforms in the Babia Góra Massif. (A) Periglacial blockfields at the Babia Góra ridge. (B) Relict pronival rampart and nivation hollow on the NE face of Mt. Diablak.

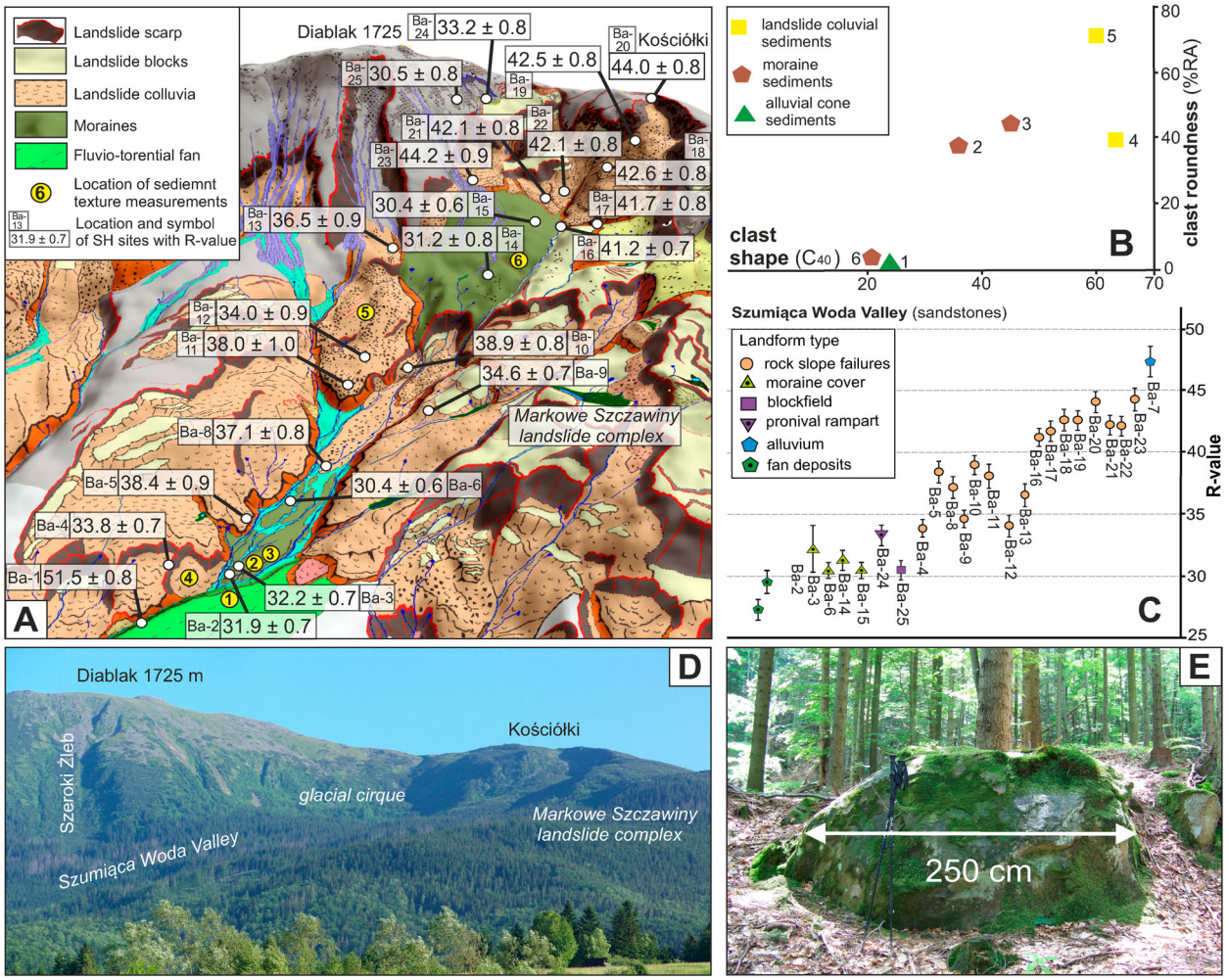

Figure 9. Glacial landforms and sediments at the Babia Góra Massif. (A) Spatial distribution of Schmidt Hammer rebound values in the Szumiąca Woda Valley plotted on the Main Map projected on the LiDAR DEM. (B) Co-variance plot for the main sediments types in the Szumiąca Woda valley. Site location showed at panel A. (C) Mean R-values with SEM intervals for the landforms in the Szumiąca Woda Valley. Numerals in the graph refer to measurement locations in panel A. R-values for the fans were adopted from Kłapyta and Kolecka (2015). (D) General view on the glacial cirque between Diablak and Kościółki Mts. (E) Large sandstone boulder at the frontal part of terminal moraine in the Szumiąca Woda Valley.

older than landslide boulders (R = 34–44) (Figure 9(a, c), Supplementary data 2).

4.3. Fluvial landforms

Impressively large fans were mapped beyond mass movement landforms at the foot of the Babia Góra Massif. They form gently inclined (5°) surfaces of well-rounded Magura sandstone clasts (5–10 cm in diameter) with a clayey-sandy matrix. Exceptionally large fans occur widely across the northern slope of the study area attaining 200 m in cone height and 1200 m in radius. An outsized fan (3.7 km in radius and 210 m hight) was also identified in the Bystrá valley on the southern foreland (out of the map). A double system of fans located at 60 m (Sulowa Cyrhel level, Middle Pleistocene) and 15–20 m (Słonowy level, Late Pleistocene) above the present floodplain was identified (Kłapyta & Kolecka, 2015). Sediment fans represent the oldest mapped landforms in the study area with the lowest recorded R-values between 27 and 29 (Kłapyta & Kolecka, 2015) (Figure 9(c)). The distal part of the Słonowy level fans passes directly into 15–10 m high river terraces (Late Pleistocene; Książkiewicz, 1963). The genesis of cone-shaped fans in the Babia Góra Massif may be complex. Prolonged incremental growth by fluvial and debris-flow processes is evidenced by layered fan sediments on the southern slope of the study area. In contrast, massive diamicton in the Cylowy fan suggests that it formed from massive slope failure and therefore represents a landslide-related fan *sensu* Sorriso-Valvo (1988). This is supported by its low fan/catchment area ratio (0.88) typical of outsize fans (Jarmann et al., 2011), derived from catastrophic slope failures. A large fan in the distal part of moraines in the Szumiąca Woda Valley could be related to glaciofluvial accumulation. The youngest set of river terraces (Rybny level, 5–6 m high) was formed during the Holocene. A total of 20 landslide lakes (largest 450–1500 m^2 in area) and two peat bogs were recognised in the Massif (Łajczak, 2016).

5. Discussion and conclusions

The Map documents the complexity of mass movements in a mountain flysch area of moderate elevation. The Babia Góra area has undergone wholesale slope modification and downwasting by having one of the highest incidences of slope failure yet recorded in Europe (29% for a whole massif, and 45% for the north face). The total area covered by RSFs is much higher than calculated for the other part of the Outer Western Carpathians (Figure 1), e.g. Moravskoslezské Beskydy Mts. (20%; Březný & Pánek, 2017), Police range (12.9%; Zatorski et al., 2017), NW part of the Beskyd Niski Mts. (22.4%; Długosz, 2011) and Czech part of the Flysch Carpathians (8%; Pánek et al., 2019). In the British mountains the maximum area affected by RSF reach 10–20% in the selected massifs (Jarman, 2006; Jarman & Harrison, 2019). Conversely, in some valleys in the Italian Alps, extraordinary concentration rock mass-wasting could reach 38% of the area (Fioraso, 2017).

Although the large RSFs constitutes first-time failures, sensu Soldati et al. (2004), they gave no evidence of a single giant rockslide on the northern slope suggested by Alexandrowicz (1978) and Ziętara (2004), that was to produce a 8 km long scarp, 200 m thick debris mass and 1 km southward retreat of the main ridge. RSF ages are unknown in the study area, however, morphological relations and SH relative age dating (Figure 9), suggest that they have evolved during or just after deglaciation and have significantly degraded glacial and periglacial relief. The remnants of moraines and glacial cirque between Diablak and Kościółki (Figure 9) indicate local glaciation of the north face of the Massif during the last glaciation (most probably the LGM) (Książkiewicz, 1963; Łajczak, 1998, 2014; Niemirowski, 1963). However, the small scale of glaciation (0.87 km^2 area, and 2.2 km glacier length) and limited glacial erosion preclude a paraglacial origin of mapped RSFs. Similarly, the fluvial pattern with low-elevated headwaters and relatively weak stream incision do not support a 'parafluvial' (Jarman et al., 2014) genesis of RSFs. Recent findings of post-LGM tectonic rupture along the southern margin of the Tatra Mountains (Pánek et al., 2020) indicate that the high-magnitude earthquakes (Mw > 7) could be possible triggers for some RSFs in the Western Carpathians. Seismic triggering related to regional-scale glacial isostatic adjustment due to the retreat of Scandinavian ice sheet (Pánek et al., 2020) is thus not ruled out as a mechanism of some RSFs in the study area. Postglacial evolution of the Babia Góra massif is possible coupled with the long-term/post-Miocene evolution of this area, which was characterised by gravitational displacement of large blocks leading to significant unloading and 'en block' uplift of the core zone of the Massif. The mechanism of footwall elevation (Wernicke & Axen, 1988) of the Babia Góra Massif along normal faults was recently proposed by Jankowski and Margielewski (2014) and Jankowski et al. (2019). In this context, the high incidences of slope failures in the study area could be related to the long-term response to uplift and thus perhaps a 'paratectonic driver'. Subsequent mass movements are recurrent features within older landforms that produced RSFs concentrated in headwater areas and on steep slopes of the cuesta, where rock avalanches were formed. SH R-values suggest its Holocene age. In order to determine timing and possible causes of RSFs in the Babia Góra Massif further

research with geophysical prospecting, kinematic analysis and cosmogenic nuclide dating should be undertaken.

Software

The software used was ESRI ArcGIS 10.6.1 to georeference, digitise, visualise the aerial photographs and generate the geomorphological map. CorelDRAW X8 was used to final map processing.

Acknowledgements

The present research work was funded by Jagiellonian University statutory grant no. DS/MND/WBiNoZ/IGiGP/5/2015 to P. Kłapyta. I wish to thank the authorities of Babia Góra National Park (Poland) for their permission to conduct research work in this protected natural area. Special thanks to J. Cząstka-Kłapyta for help in the fieldwork. Thanks to the four Referees: Dr David Jarman, Dr Mike Shand, Dr Jan Lenart and Dr Raul-David Serban for their valuable and thorough reviews and useful comments, from which I have greatly benefited in revising the manuscript and the geolmorphological map.

Disclosure statement

No potential conflict of interest was reported by the author(s).

ORCID

Piotr Kłapyta http://orcid.org/0000-0001-6853-4074

References

Agliardi, F., Crosta, G. B., & Zanchi, A. (2001). Structural constrains on deep-seated slope deformations kinematics. *Engineering Geology*, *59*(1–2), 83–102. https://doi.org/10.1016/S0013-7952(00)00066-1

Aleksandrowski, P. (1985). Tektonika region babiogórskiego: interferencja zachodnio i wschodniokarpackich kierunków fałdowych. *Annales Societates Geologorum Poloniae*, *5*(3–4), 375–422.

Alexandrowicz, S. W. (1978). The northern slope of Babia Góra Mt. as a huge rock slump. *Studia Geomorphologica Carpatho-Balcanica*, *12*, 133–148.

Alexandrowicz, S. W. (2004). Outlines of geology of the Babia Góra range. In B. W. Wołoszyn, A. Jaworski, & J. Szwagrzyk (Eds.), *The nature of the Babiogórski National Park* (pp. 87–107). Komitet Ochrony Przyrody PAN, Babiogórski Park Narodowy, Kraków.

Benn, D. I., & Ballantyne, C. K. (1994). Reconstructing the transport history of glacigenic sediments: A new approach based on the co-variance of clast form indices. *Sedimentary Geology*, *91*(1–4), 215–227. https://doi.org/10.1016/0037-0738(94)90130-9

Březný, M., & Pánek, T. (2017). Deep-seated landslides affecting monoclinal flysch morphostructure: Evaluation of LiDAR-derived topography of the highest range of the Czech Carpathians. *Geomorphology*, *285*, 44–57. https://doi.org/10.1016/j.geomorph.2017.02.007

Cruden, D. M., & Varnes, D. J. (1996). Landslide types and processes. In A. K. Turner & R. L. Shuster (Eds.), *Landslides: Investigation and Mitigation* (pp. 36–75). Transportation Research Board.

Czajka, B., Łajczak, A., & Kaczka, R. J. (2015). The dynamics of the timberline ecotone on the asymmetric ridge of the Babia Góra Massif, Western Carpathians. *Geographia Polonica*, *88*(2), 85–102. https://doi.org/10.7163/GPol.0017

Długosz, M. (2011). Podatność stoków na osuwanie w polskich Karpatach Fliszowych. Prace Geograficzne IG i PZ PAN, 230,Warszawa.

Dobiński, W., Glazer, M., Bieta, B., & Mendecki, M. J. (2016). Poszukiwanie wieloletniej zmarzliny i budowa geologiczna Babiej Góry w świetle wyników obrazowania elektrooporowego. *Przegląd Geograficzny*, *88*(1), 31–51. https://doi.org/10.7163/PrzG.2016.1.2

ESRI. (2016). Terrain Tools Sample v1.1. A suite of Geoprocessing tools to produce cartographic effects for terrain representation.

Fell, R. (1994). Landslide risk assessment and acceptable risk. *Canadian Geotechnical Journal*, *31*(2), 261–272. https://doi.org/10.1139/t94-031

Fioraso, G. (2017). Impact of massive deep-seated rock slope failures on mountain valley morphology in the northern Cottian Alps (NW Italy). *Journal of Maps*, *13*(2), 575–587. https://doi.org/10.1080/17445647.2017.1342211

Golonka, J., & Wójcik, A. (1976). *Szczegółowa mapa geologiczna Polski 1:50 000, arkusz Jeleśnia*. Wydawnictwo Geologiczne.

Heyman, B. M., Heyman, J., Fickert, T., & Harbor, J. M. (2013). Paleo-climate of the central European uplands during the last glacial maximum based on glacier mass-balance modelling. *Quaternary Research*, *79*(1), 49–54. https://doi.org/10.1016/j.yqres.2012.09.005

Jahn, A. (1958). Mikrorelief peryglacjalny Tatr i Babiej Góry. *Biuletyn Peryglacjalny*, *6*, 57–80.

Jankowski, L., & Margielewski, W. (2014). Strukturalne uwarunkowania rozwoju rzeźby Karpat zewnętrznych–nowe spojrzenie. *Przegląd Geologiczny*, *62*(1), 29–35.

Jankowski, L., Margielewski, W., Garecka, M., & Kowalska, S. (2019). Skalisty fragment koryta Skawicy w Zawoi z asocjacją różnowiekowych uskoków. In L. Jankowski (Ed.), *Od podnóża Tatr po brzeg Karpat, Współczesne wyzwania kartografii geologicznej, Conference Materials* (pp. 59–65). Państwowy Instytut Geologiczny.

Jarman, D. (2006). Large rock slope failures in the Highlands of Scotland: Characterisation, causes and spatial distribution. *Engineering Geology*, *83*(1-3), 161–182. https://doi.org/10.1016/j.enggeo.2005.06.030

Jarman, D., Calvet, M., Corominas, J., Delmas, M., & Gunnell, Y. (2014). Large-scale rock slope failures in the eastern Pyrenees: Identifying a sparse but significant population in paraglacial and parafluvial contexts. *Geografiska Annaler: Series A, Physical Geography*, *96*(3), 357–391. https://doi.org/10.1111/geoa.12060

Jarman, D., & Harrison, S. (2019). Rock slope failure in the British mountains. *Geomorphology*, *340*, 202–233. https://doi.org/10.1016/j.geomorph.2019.03.002

Jarmann, D., Agliardi, F., & Crosta, G. B. (2011). Megafans and outsize fans from catastrophic slope failures in Alpine glacial troughs: the Malser Haide and the Val Venosta cluster, Italy. In: M. Jaboyedoff (Eds.), *Slope Tectonics*, Geological Society, Special Publications, 351, 253–277.

Kirkbride, M. P., & Winkler, S. (2012). Correlation of Late Quaternary glacier chronologies: Impact of climate

variability, glacier response, and chronological resolution. *Quaternary Science Reviews*, *46*, 1–29. https://doi.org/10.1016/j.quascirev.2012.04.002

Klimaszewski, M. (1948). *Polskie Karpaty Zachodnie w okresie dyluwialnym*. Prace Wrocławskiego Towarzystwa Naukowego, 7.

Klimaszewski, M. (1952). Zagadnienia plejstocenu południowej Polski. *Biuletyn Państwowego Instytutu Geologicznego*, *65*, 137–268.

Kłapyta, P. (2013). Application of Schmidt hammer relative age dating to Late Pleistocene moraines and rock glaciers in the Western Tatra Mountains, Slovakia. *Catena*, *111*, 104–121. https://doi.org/10.1016/j.catena.2013.07.004

Kłapyta, P., & Kolecka, N. (2015). Combining LiDAR data with field mapping and Schmidt-hammer relative age dating – examples from the Babia Góra range (Western Carpathians, Poland). In: J. Jasiewicz, Z. Zwoliński, H. Mitasova, & T. Hengl (Eds.), *Geomorphometry for geosciences* (pp. 217–220), Poznań.

Książkiewicz, M. (1963). Zarys geologii Babiej Góry. *Zakład Ochrony Przyrody PAN*, *22*, 69–87.

Książkiewicz, M. (1966). *Geologia regionu babiogórskiego*. Przewodnik XXXIX Zajadu Polskiego Towarzystwa Geologicznego, 5–59.

Książkiewicz, M. (1971). *Szczegółowa mapa geologiczna Polski 1:50 000, arkusz Zawoja*. Instytut Geologiczny.

Książkiewicz, M. (1983). The geology of the Babia Góra region. In: K. Zabierowski (Ed.), National Park on the Babia Góra Mt. Nature and Man. Studia Naturae B 29, 25–39.

Łajczak, A. (1998). *Distribution of glacial and nival forms in the Babia Góra Massif, Western Carpathians*. Proceedings of the 4th Meeting of Polish Geomorphologists Part II, Lublin: 349–356.

Łajczak, A. (2013). Relief development of a highly elevated monoclinal Babia Góra range built by Magura sandstone, Western Carpathian Mts. In: P. Migoń, M. Kasprzak (Eds.), *Sandstone landscapes. Diversity, ecology and conservation*. Proc. of Wrocław University: 100–105.

Łajczak, A. (2014). Relief development of the Babia Góra Massif, Western Carpathian mountains. *Quaestiones Geographicae*, *33*(1), 89–106. https://doi.org/10.2478/quageo-2014-0006.

Łajczak, A. (2016). *Wody Babiej Góry. Monografie Babiogórskie*. Babiogórski Park Narodowy, Homago Studio Graficzne, Maków Podhalański.

Łajczak, A., Czajka, B., & Kaczka, R. J. (2014). The new features of landslide relief discovered using LiDAR – case study from Babia Góra massif, Western Carpathian mountains. *Quaestiones Geographicae*, *33*(3), 77–88. https://doi.org/10.2478/quageo-2014-0031

Łajczak, A., Czajka, B., & Kaczka, R. J. (2015). Development of tourist infrastructure on Babia Góra Mt. (Western Carpathians) in conditions where there is risk due to slope processes. *Prace Geograficzne*, *142*, 7–40.

Łajczak, A., & Migoń, P. (2002). The 2002 debris flow in the Babia Góra Massif – Implications for the interpretation of mountainous Geomorphic systems. *Studia Geomorphologica Carpatho-Balcanica*, *51*, 97–116.

Łajczak, A., & Włoch, E. (2004). Gołoborza na Babiej Górze i ich znaczenie paleogeograficzne. In: Łajczak A. (Ed.) *Pokrywy stokowe gór średnich strefy umiarkowanej i ich znaczenie paleogeograficzne*. Warsztaty Geomorfologiczne, Zawoja.

Margielewski, W. (2006a). Structural control and types of movements of rock mass in anisotropic rocks: Case studies in the Polish Flysch Carpathians. *Geomorphology*, *77*(1-2), 47–68. https://doi.org/10.1016/j.geomorph.2006.01.003

Margielewski, W. (2006b). Records of the Late Glacial–Holocene palaeoenvironmental changes in landslide forms and deposits of the Beskid Makowski and Beskid Wyspowy Mt area (Polish Outer Carpathians). *Folia Quaternaria*, *76*, 1–149.

Matthews, J. A., & Shakesby, R. A. (1984). The status of the "Little Ice Age" in southern Norway: Relative dating of Neoglacial moraines with Schmidt Hammer and lichenometry. *Boreas*, *13*(3), 333–346. https://doi.org/10.1111/j.1502-3885.1984.tb01128.x

Matyja, M. (2006). The significance of trees and coarse debris in shaping the debris flow accumulation zone (north slope of the Babia Góra Massif, Poland). *Geographia Polonica*, *80*(1), 83–99.

Midowicz, W. (1974). Babia Góra. *Monografia turystyczna. Karpaty*, *2*, 61–96.

Mrozek, T., Kułak, M., Grabowski, M., & Wójcik, A. (2014). Landslide counteracting system (SOPO): inventory database of landslides in Poland. In K. Sassa, P. Canuti, & Y. Yin (Eds.), *Landslide Science for a Safer Geoenvironment* (pp. 815–820). Springer.

Němčok, A. (1982). *Zosuvy v slovenských Karpatoch*. VEDA.

Niemirowski, M. (1963). Szkic geograficzny obszaru babiogórskiego. *Zakład Ochrony Przyrody PAN*, *22*, 21–43.

Obrębska-Starklowa, B. (2004). Klimat masywu Babiej Góry. In: B. W. Wołoszyn, A. Jaworski, J. Szwagrzyk(Eds.). *Babiogórski Park Narodowy—monografia przyrodnicza* (pp. 137–151). Komitet Ochrony Przyrody PAN, Babiogórski Park Narodowy.

Ondrášik, R. (2002). Landslides in the West Carpathians. In: J. Rybář, J. Stemberk, P. Wagner (Eds.), *Landslides* (pp. 45–57).

Pánek, T., Břežný, M., Kapustová, V., Lenart, J., & Chalupa, V. (2019). Large landslides and deep-seated gravitational slope deformations in the Czech Flysch Carpathians: New LiDAR-based inventory. *Geomorphology*, *346*, 106852. https://doi.org/10.1016/j.geomorph.2019.106852

Pánek, T., Engel, Z., Mentlík, P., Braucher, R., Břežný, M., Škarpich, V., & Zondervan, A. (2016). Cosmogenic age constraints on post-LGM catastrophic rock slope failures in the Tatra Mountains (Western Carpathians). *Catena*, *138*, 52–67. https://doi.org/10.1016/j.catena.2015.11.005

Pánek, T., & Klimeš, J. (2016). Temporal behavior of deep-seated gravitational slope deformations: A review. *Earth-Science Reviews*, *156*, 14–38. https://doi.org/10.1016/j.earscirev.2016.02.007

Pánek, T., Minár, J., Vitovič, L., & Břežný, M. (2020). Post-LGMfaulting in Central Europe: LiDAR detection of the >50 km-long Sub-Tatra fault, Western Carpathians. *Geomorphology*, *364*, 107248. https://doi.org/10.1016/j.geomorph.2020.107248

Pánek, T., Smolková, V., Hradecký, J., Baroň, I., & Šilhán, K. (2013). Holocene reactivations of catastrophic complex flow-like landslides in the Flysch Carpathians (Czech Republic/Slovakia). *Quaternary Research*, *80*(1), 33–46. https://doi.org/10.1016/j.yqres.2013.03.009

Rehman, A. (1895). *Opis fizyczno-geograficzny ziem polskich i sąsiednich krajów słowiańskich. Opis fizyczno-geograficzny Karpat*.

Sawicki, L. (1913). Krajobrazy lodowcowe Zachodniego Beskidu. *Rozprawy Wydziału Matematyczno-Przyrodniczego PAU*, *53*, 1–21.

Shakesby, R. A., Matthews, J. A., & Owen, G. (2006). The Schmidt hammer as a relative-age dating tool and its potential for calibrated-age dating in Holocene glaciated environments. *Quaternary Science Reviews*, *25*(21-22), 2846–2867. https://doi.org/10.1016/j.quascirev.2006.07.011

Soldati, M., Corsini, A., & Pasuto, A. (2004). Landslides and climate change in the Italian Dolomites. *Catena*, *55*(2), 141–161. https://doi.org/10.1016/S0341-8162(03)00113-9

Sorriso-Valvo, M. (1988). Landslide-related fans in Calabria. *Catena Supplement*, *13*, 109–121.

Starkel, L. (1960). *Rozwój rzeźby Karpat fliszowych w holocenie*. Prace Geograficzne IG PAN, 22.

Teťák, F., Kováčik, M., Pešková, I., Nagy, A., Buček, S., Maglay, J., & Vlačiky, M. (2016). *Geologická mapa regiónu Biela Orava v mierke 1 : 50 000*. MŽP SR/ŠGÚDŠ, Bratislava.

Van Den Eeckhaut, M., Kerle, N., Poesen, J., & Hervás, J. (2012). Object-oriented identification of forested landslides with derivates of single pulse LiDAR data. *Geomorphology*, *173–174*, 30–42. https://doi.org/10.1016/j.geomorph.2012.05.024

Wernicke, B., & Axen, G. J. (1988). On the role of isostasy in the evolution of normal fault system. *Geology*, *16*(9), 848–851. https://doi.org/10.1130/0091-7613(1988)016<0848:OTROII>2.3.CO;2

Wójcik, A., Rączkowski, W., Mrozek, T., Nescieruk, P., Marciniec, P., & Zimnal, Z. (2010). *Babiogórski Park Narodowy 1 : 13 000*. Ministerstwo Środowiska, Warszawa.

Zapałowicz, H. (1880). *Roślinność Babiej Góry pod względem geograficzno-biologicznym*. Sprawozdanie Komisji Fizjograficznej AU, 14. 79–236.

Zatorski, M., Franczak, P., Buczek, K., Strzyżowski, D., & Witkowski, K. (2017). Rzeźba terenu i jej współczesne przemiany. In: P. Franczak (Eds.) *Police* (pp. 31–64). Pasmo w cieniu Babiej Góry, IGiGP UJ.

Ziętara, K., & Ziętara, T. (1958). *O rzekomo glacjalnej rzeźbie Babiej Góry*. Rocznik Naukowo-Dydaktyczny WSP, Geografia, 8, 55–78.

Ziętara, T. (1962). *O pseudoglacjalnej rzeźbie Beskidów Zachodnich*. Rocznik Naukowo-Dydaktyczny WSP, Geografia, 10, 69–87.

Ziętara, T. (1989). Rozwój teras krioplanacyjnych w obrębie wierzchowiny Babiej Góry w Beskidzie Wysokim. *Folia Geographica, ser. Geographia Physica*, *21*, 79–92.

Ziętara, T. (2004). *Rzeźba Babiej Góry*. In: B. W. Wołoszyn, A. Jaworski, J. Szwagrzyk (Eds.), *Babiogórski Park Narodowy—monografia przyrodnicza* (109–135), Komitet Ochrony Przyrody PAN, Babiogórski Park Narodowy.